Current-voltage relation for the Saturnian system

L. C. Ray,[1,2] M. Galand,[1] P. A. Delamere,[3] and B. L. Fleshman[4]

Received 8 January 2013; revised 9 April 2013; accepted 9 May 2013.

[1] Saturn's magnetosphere is populated by plasma created from neutrals ejected by the moon Enceladus. These neutrals are ionized and picked up by the planetary magnetic field requiring large amounts of angular momentum to be transferred from Saturn's upper atmosphere to the magnetospheric plasma. The resulting upward currents that supply this angular momentum are associated with electrons, which travel toward the planetary atmosphere. At high magnetic latitudes along the flux tube, parallel electric fields may develop to enhance the field-aligned current density flowing between the two regions. We show that, similar to the Jovian system, the current-voltage relation in the Saturnian system must be evaluated at the top of the acceleration region, which occurs at ~1.5 R_S along the magnetic field line as measured from the center of the planet. Owing to the large abundance of protons in the Saturnian system, cold electrons carry the majority of the field-aligned current for net potential drops less than 500 V. For the flux tube intersecting the equatorial plane at 4 R_S, field-aligned potentials of 50–130 V are consistent with the energy fluxes inferred from the Enceladus emission. In the middle magnetosphere, field-aligned potentials of ~1.5 kV produce ionospheric electron energy fluxes of 0.3 mW/m^2 when hot electrons comprise 0.3% of the magnetospheric electron population.

Citation: Ray, L. C., M. Galand, P. A. Delamere, and B. L. Fleshman (2013), Current-voltage relation for the Saturnian system, *J. Geophys. Res. Space Physics*, *118*, doi:10.1002/jgra.50330.

1. Introduction

[2] Planetary auroral emissions are the signature of magnetosphere-ionosphere coupling. At Earth, magnetosphere-ionosphere coupling can be studied through a variety of measurements and techniques: satellites such as FAST, Polar, Cluster, Themis, along with sounding rockets, make in situ measurements of energetic particles and magnetic and electric fields, while ground-based radars measure the plasma density, drift speed, and ionospheric temperature through remote sensing. Additionally, spectroscopic observations of the aurora from space (e.g., ultra-violet, V-ray wavelengths) and ground-based observations (e.g., visible, radio) provide insight into the phenomenology of the terrestrial aurora [see reviews by *Galand and Chakrabarti*, 2002; *Paschmann et al*., 2003].

[3] At Saturn, diagnostics for magnetosphere-ionosphere coupling are limited to remote sensing of auroral emissions from Earth and spacecraft measurements. While a number of spacecraft have flown by Saturn, and Cassini has been in orbit since 2004, in situ particle and field measurements have thus far been primarily limited to equatorial regions. In 2008, Cassini entered a period of high-latitude orbits; however, the too large radial distance of the spacecraft from Saturn prevented direct measurement of the auroral acceleration region.

[4] It is possible, though, to match in situ magnetospheric measurements with phenomena observed at the planetary atmosphere through use of magnetic field models [*Connerney et al*., 1983; *Dougherty et al*., 2004; *Alexeev et al*., 2006]. For example, *Bunce et al*. [2008] used Cassini measurements, along with Hubble Space Telescope (HST) observations of Saturn's ultra-violet aurora, to determine that the noon aurora marks the boundary of the open and closed field lines in Saturn's magnetosphere.

[5] There are also auroral emissions that are magnetically conjugate with equatorial regions well inside the Saturnian magnetopause. Using the HST Advanced Camera for Surveys, *Grodent et al*. [2008] found an emission equatorward of the main auroral emission on the nightside limb, which is magnetically conjugate with equatorial distances between 4 and 11 R_S. The incident energy flux associated with this emission was estimated to be ~0.3 mW/m^2. A possible driving mechanism for this emission is pitch angle scattering of the hot, magnetospheric electron population. However, this interpretation relies on our understanding of the magnetospheric environment between 4 and 11 R_S. The electron population inferred from Cassini Electron Spectrometer (ELS) measurements in this region depends on the calibration of the instrument. For instance,

[1]Department of Physics, Space, and Atmospheres Group, Imperial College London, London, UK.
[2]Now at Department of Physics and Astronomy, University College London, London, UK.
[3]Geophysical Institute, University of Alaska Fairbanks, Fairbanks, Alaska, USA.
[4]Homer L. Dodge Department of Physics and Astronomy, University of Oklahoma, Norman, Oklahoma, USA.

Corresponding author: L. C. Ray, Department of Physics, Space, and Atmospheres Group, Imperial College London, South Kensington Campus, Prince Consort Road, London SW7 2AZ, UK. (l.ray@imperial.co.uk)

2169-9380/13/10.1002/jgra.50330

Schippers et al. [2012] found the electron population from 5 to 9 R_S to be composed of cold (1–10 eV), warm (10–400 eV), and hot (400 eV–26 keV) components, compared to a cold (~5 eV) and hot (~2.4 keV) population at 9 R_S [*Schippers et al*., 2008] determined prior to the recalibration of ELS that corrected for the spacecraft potential [*Lewis et al*., 2010].

[6] Using Cassini UVIS observations, *Pryor et al*. [2011] detected an auroral spot in Saturn's atmosphere, which is located at the foot of the Enceladus flux tube. Unlike Jupiter's moon, Io, which creates an ever-present, bright auroral emission observable from HST as it moves through the local plasma environment, the Enceladus-related emission is too faint to be detected from HST [*Wannawichian et al*., 2008]. Indeed, the Enceladus emission seen by UVIS is not detectable at all times and, when visible, has a brightness ranging from 450 ± 290 Rayleighs to 1550 ± 340 Rayleighs [*Pryor et al*., 2011]. It is not possible to infer the energy of the precipitating auroral electrons from observations, owing to a lack of hydrocarbon absorption in the Enceladus spot region.

[7] In addition to the UV auroral emissions equatorward of the main auroral oval, there are also infrared (IR) auroral emissions at mid-latitudes. On the nightside of Saturn, the IR main oval splits into multiple arcs [*Stallard et al*., 2008], coincident with the UV auroral emission observed by *Grodent et al*. [2010] at ~70°. At lower latitudes, there is a second IR oval that is magnetically conjugate with the equatorial region located at 3–4 R_S [*Stallard et al*., 2010]. This location corresponds to the magnetospheric region with the largest observed lag from planetary corotation.

[8] In a steady-state, upward auroral current region, the primary acceleration mechanism for electrons is parallel electric fields. At Earth, this has been measured by satellites [*Mozer and Kletzing*, 1998; *Ergun et al*., 1998; *McFadden et al*., 1999] and inferred by sounding rocket observations in auroral regions [*Mella et al*., 2011]. The relationship between parallel electric fields and field-aligned current density was first explored by *Knight* [1973] for the terrestrial magnetosphere for a Maxwellian distribution of plasma in a monotonically increasing electric potential structure. *Lyons* [1980] extended the *Knight* [1973] analysis to find that the relationship between the field-aligned current density and parallel electric field strength is linear when the mirror ratio, R_x, between the top of the acceleration region and the planetary atmosphere is much larger than the ratio between the energy of the potential drop, $e\Phi$, and the average thermal energy of the electron distribution, kT_e, i.e., $1 << \frac{e\Phi}{kT_e} << R_x$. *Dors and Kletzing* [1999] derived a current-voltage relationship for a Kappa distribution of particles, finding that the presence of a high-energy electron population decreased the magnitude of the saturation current density in the system and increased the incident energy flux into the planetary atmosphere. *Boström* [2003] derived a current-voltage relation for a magnetic flux tube under more general conditions, using kinetic "orbital motion" theory. He found that the total voltage drop along a flux tube is uniquely determined by the current density as long as particles do not mirror due to local maxima in the effective field-aligned potential. When particles are mirrored by a local maximum in the effective potential, the solution method must take into account the spatial distribution of charged particles and solve the Poisson equation to determine the potential structure along the flux tube. In that case, the relationship between the total voltage drop and current is nonunique. However, none of the aforementioned analytic studies explicitly investigated how the presence of ambipolar electric fields would affect the current-voltage relation.

[9] Earth's rotation rate is relatively slow. The plasma distribution along a flux tube is largely dictated by gravitational and mirror forces. As a consequence, the density decreases along the magnetic field lines toward the equatorial plane. However, at Saturn, large centrifugal forces stemming from the rapid planetary rotation rate of ~10.6 h result in an equatorial plasma sheet. Cold, dense, and positively charged water group ions are confined to the equator [*Sittler et al*., 2008; *Thomsen et al*., 2010], while lighter electrons and protons move more freely along the field. The resulting charge separation produces an ambipolar electric field that pulls the protons off the equator and hinders the motion of the electrons toward the ionosphere.

[10] *Ergun et al*. [2000] developed a static 1-D spatial 2-D velocity space Vlasov code to model the potential structure in the upward current region at Earth, finding good agreement with FAST data. *Su et al*. [2003] modified this model to include the large centrifugal forces in the Jovian magnetosphere. Their analysis investigated how the potential structure of the Io flux tube and ionospheric current density varied with the composition of the Io plasma torus. *Su et al*. [2003] found that the strength of the ambipolar potential varied inversely with the abundance of light ions (e.g., H^+) in the Io torus. Additionally, the current density at high latitudes was found to be strongly dependent on the hot electron population owing to the large ambipolar potentials.

[11] *Ray et al*. [2009] extended the *Su et al*. [2003] analysis to explore the current-voltage relation in the Jovian system, where a minimum in the sum of the centrifugal and gravitational forces leads to a reduction of the plasma density at high latitudes. Their analysis showed that the *Knight* [1973] current-voltage relation is appropriate for centrifugally confined systems, provided that the plasma parameters, mirror ratios, and potentials are evaluated at the top of the acceleration region, which exists at 2–3 Jovian radii along the magnetic field as measured from the center of the planet.

[12] In this study, we extend the *Ray et al*. [2009] analysis to the Saturnian magnetosphere. *Ray et al*. [2012] showed that Saturn's lower mass and larger abundance of light ions in the magnetospheric plasma, owing to Enceladus's water-based chemistry rather than Io's sulfur-dioxide based chemistry, yields smaller ambipolar electric fields than in the Jovian system. Additionally, they showed that the ionospheric current density and precipitating electron energy flux vary strongly with the density and temperature of the magnetospheric plasma population. We suggest that field-aligned potentials may be necessary to provide the field-aligned currents that transfer angular momentum from Saturn's upper atmosphere to its magnetospheric plasma for magnetospheric plasma populations with a small fraction of hot electrons [*Schippers et al*., 2012]. If this is the case, then field-aligned potentials may be responsible for the emissions observed by *Stallard et al*. [2010] and *Grodent et al*. [2010]. Therefore, it is necessary to understand the behavior of the current-voltage relation in Saturn's middle magnetosphere, specifically the location along the magnetic flux tube at which the current-voltage relation should be evaluated.

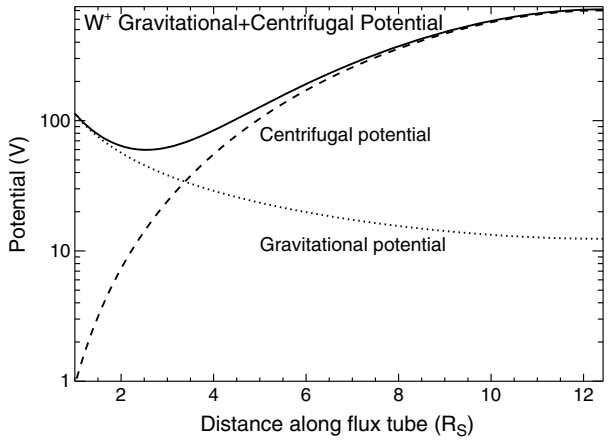

Figure 1. Gravitational and centrifugal potentials for water group ions along the flux tube mapping to 9 R_S in the equatorial plane. The ionospheric end of the flux tube is on the left, and the magnetospheric end is on the right. The minimum in the sum of the potentials exists at ~2.5 R_S along the field above the ionosphere.

[13] The most complete electron data analysis exists at 9 R_S, coincident with the magnetically conjugate location of the diffuse auroral emission. We therefore focus our analysis on the flux tube which intersects the equatorial plane at this location. We also explore the current-voltage relation for the Enceladus flux tube at 4 R_S with an aim at parameterizing the strength of field-aligned potentials that would produce the observed auroral emissions. Section 2 briefly describes our model. In section 3, we detail the boundary conditions and initial assumptions, along with our model outputs. We compare our results to existing analytic current-voltage relations in section 4. Finally, we discuss our results in comparison with observations in section 5 and conclude in section 6.

2. Model Description

[14] We use a steady-state kinetic Vlasov code [*Ergun et al*., 2000; *Su et al*., 2003; *Ray et al*.,2009, 2012] to determine the field-aligned density, potential structure, and ionospheric field-aligned current density for the flux tubes intersecting the equatorial plane at 4 R_S and 9 R_S, corresponding to planetary latitudes of $-62.1°$ and $-70°$, respectively. The reader is referred to *Ray et al*. [2012] for a detailed description of the Vlasov model as applied to Saturn.

[15] In brief, the Vlasov solver is 1-D spatially, along a magnetic field line, and 2-D in velocity space. The magnetic field is defined by the *Dougherty et al*. [2005] internal field model plus the ring current field described by *Bunce et al*. [2007] with an average subsolar magnetopause distance of 25 R_S [*Achilleos et al*., 2008]. The spatial domain is divided into N_S grids that are evenly spaced along the magnetic field line where $N_S = 51$ (~0.1 R_S) and $N_S = 61$ (~0.2 R_S) for the flux tubes intersecting 4 R_S and 9 R_S, respectively.

[16] The Vlasov model includes gravitational, centrifugal, and mirror forces. Figure 1 displays the gravitational and centrifugal potentials for water group ions along the magnetic field line mapping to 9 R_S in the equatorial plane. The boundary conditions are the plasma properties at the ionospheric and magnetospheric ends of the flux tube and the net potential drop between the two regions. Plasma populations are defined either as Boltzmann, Kappa, or Maxwellian distributions. Kappa and Maxwellian distributions are broken into $N_v \times N_v$ velocity-space elements ($N_v = 100$) that are initialized at the magnetospheric boundary and are then calculated at each spatial location along the flux tube. Boltzmann populations are treated in a fluid manner, varying spatially as $n_{Boltz}(s) = n_0 e^{(-\Phi_{\mathrm{Tot}}(s)/T_0)}$ where T_0 and n_0 are the temperature and density of the species in the equatorial plane, and $\Phi_{\mathrm{Tot}}(s)$ is the field-aligned potential structure given by the sum of the gravitational, centrifugal, and electric potentials.

[17] To solve for the field-aligned current density, the net potential drop between the ionosphere and the equatorial magnetosphere must be user specified. We vary it in this analysis to derive a current-voltage relation for the Saturnian system. Plasma is distributed along the magnetic field lines with the Vlasov code, which uses conservation of energy and the first adiabatic invariant. The field-aligned potential is held fixed at the ionospheric and equatorial magnetospheric ends of the magnetic flux tube; however, the spatial structure of the potential along the field is modified solving Poisson's equation at each spatial step to calculate the error, $\xi(s)$

$$\xi(s) = \nabla^2\Phi(s) + \frac{e}{\epsilon_0}[n_i(s) - n_e(s)] \quad (1)$$

where e is the charge of the electron, ϵ_0 is the permittivity of free space, and $n_i(s)$ and $n_e(s)$ are the ion and electron densities along the flux tube, respectively, as calculated from the distribution functions. We iteratively adjust the electric potential, $\Phi(s)$, to minimize the total error $\int \xi(s) ds$, yielding a steady-state solution along the magnetic field line. As the centrifugal and gravitational forces are dictated by physical properties of Saturn, changes in the field-aligned potential reflect modifications to the ambipolar potential. The spatial size of the grid ($ds \sim 10{,}000$ km) is significantly larger than the Debye length ($\lambda_D < 1$ km); hence, the first term on the right-hand side of equation (1) is negligible, essentially resulting in a quasi-neutral solution. Once a quasi-neutral solution is determined, we then calculate the incident electron energy flux into the ionosphere.

3. Vlasov Solutions

[18] The equatorial and ionospheric plasma compositions are held fixed for each flux tube while we vary the net potential drop between the ionosphere and the magnetosphere. Therefore, any changes in the field-aligned current density attest to a variation in the net field-aligned potential drop.

Table 1. Plasma Compositions, Temperatures, and Distribution Types Set at the Ionospheric and Magnetospheric Boundaries for Case of the Flux Tube Intersecting 4 R_S

Species	Density (cm^{-3})	Temp. (eV)	Type
Iono. H^+	2×10^4	0.059	Boltzmann
Iono. e^-	2×10^4	0.059	Boltzmann
Mag. W^+	55	30 ; $\frac{T_\perp}{T_\parallel} = 5$	Maxwellian
Mag. H^+	5	4	Boltzmann
Mag. e^-	60	5	Kappa, $\kappa = 3$

Table 2. Plasma Compositions, Temperatures, and Distribution Types set at the Ionospheric and Magnetospheric Boundaries for Case of the Flux Tube Intersecting 9 R_S

Species	Density (cm^{-3})	Temp. (eV)	Type
Iono. H^+	2×10^4	0.059	Fluid
Iono. e^-	2×10^4	0.059	Fluid
Mag. W^+	4.62	165.0 ; $\frac{T_\perp}{T_\parallel} = 2$	Maxwellian
Mag. H^+	0.66	27.0	Boltzmann
Mag. e^-_h	0.02	1000.0	Maxwellian
Mag. e^-_c	5.26	6.0	Kappa, $\kappa = 1.97$

Tables 1 and 2 show the ionospheric and magnetospheric boundary conditions for flux tubes intersecting 4 R_S and 9 R_S, respectively. Ionospheric plasma properties are from the analysis of *Kliore et al*. [2009]. The magnetospheric plasma composition in the equatorial plane for the 4 R_S case is based on the best-fit parameters from the physical chemistry model of *Fleshman et al*. [2010]. For the 9 R_S case, the ion properties follow the analysis of *Wilson et al*. [2008], and the electron properties are from the analysis of *Schippers et al*. [2012]; however, the ion densities from *Wilson et al*. [2008] have been modified such that the magnetospheric population is quasi-neutral. Unless otherwise stated, we focus on the flux tube intersecting the equatorial plane at 9 R_S from hereafter, as the results for the 4 R_S and 9 R_S cases are qualitatively similar.

[19] From top to bottom, Figure 2 shows the field-aligned densities, field-aligned potential structure, and ambipolar potentials for a net potential drop of 100 V along the flux tube intersecting the equatorial plane at 9 R_S. The green, blue, black, and red lines represent magnetospheric cold electrons, water group ions, protons, and hot electrons, respectively. Ionospheric protons and electrons are shown in pink and orange. The magnetospheric proton and hot electron densities remain nearly constant along the field line. Water group ions have limited field-aligned mobility, with their density decreased by an order of magnitude ~2 R_S above the equatorial plane. The cold electron density also falls off with distance along the magnetic field line, matching that of the protons at midlatitudes. A narrow density cavity, spanning ~0.3 R_S, is apparent at ~1.5 R_S along the magnetic field as measured from the center of the planet. This is near the location where the minimum in the sum of the gravitational and centrifugal potentials exists and coincides with a sharp drop in the field-aligned potential. The magnitude of this drop is the net potential difference between the ionosphere and magnetosphere, plus the magnetospheric ambipolar potential less the ionospheric ambipolar potential.

[20] The profiles displayed in Figure 2 are characteristic of all runs with the sharp potential drop consistently located near the minimum in the sum of the gravitational and centrifugal potentials, where a natural minimum in the plasma density occurs. The magnitude of the magnetospheric ambipolar potential depends on the centrifugal force and

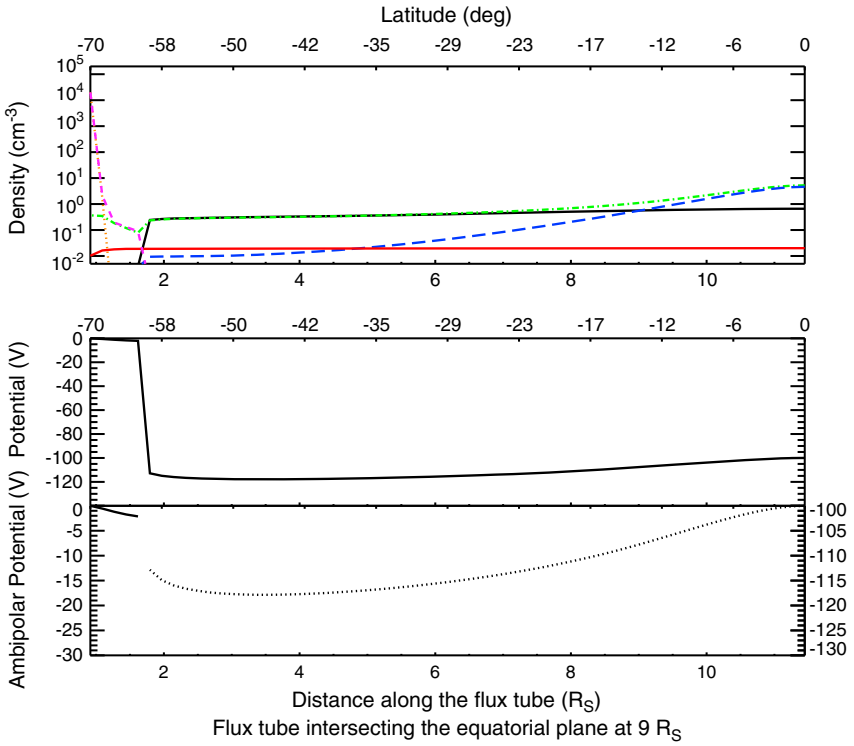

Figure 2. Plasma density, field-aligned potential, and ambipolar potential profiles along the magnetic flux tube mapping to 9 R_S. The plasma species are magnetospheric cold electrons (green, dot-dashed line), water group ions (blue, long dashed line), protons (black, solid) and hot electrons (red, dot-dot-dot-dashed line), and ionospheric protons (pink, short dashed line) and electrons (orange, dotted line). The scale on the right-hand side of bottom panel reflects the net potential difference of 100 V between the ionosphere and magnetosphere.

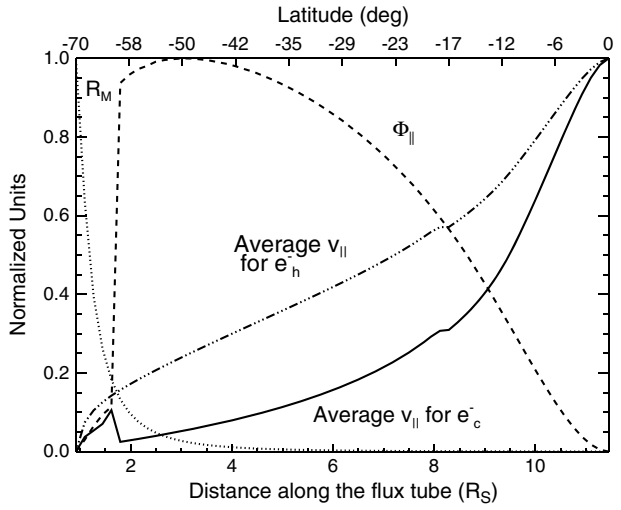

Figure 3. Normalized field-aligned properties for the flux tube mapping to 9 R_S with a 0 V net potential drop between the ionosphere and magnetosphere. The solid and dash-dot-dot-dot lines are the normalized average parallel velocities of the cold and hot electron distributions, respectively. The dashed line is the normalized field-aligned potential, and the dotted line is the normalized mirror ratio along the field. Note the sharp jump in the average parallel velocity of the cold electrons at the same location as the potential drop. The kink in the average velocities at ~8.2 R_S is reflects the boundary of the magnetospheric current sheet in the magnetic field structure.

the energy of the magnetospheric plasma population. Therefore, in this analysis, the structure of the ambipolar potential on the magnetospheric side of the potential drop does not vary with net potential drop, except for the baseline magnitude. Just on the magnetospheric edge of the potential drop, the magnitude of the magnetospheric ambipolar potential decreases slightly. However, this is small compared to the maximum magnetospheric ambipolar potential. Therefore, even in the case of a 0 V net potential drop, high-latitude electrons experience a field-aligned acceleration, the strength of which is the difference between the magnetospheric and ionospheric ambipolar potentials, less the small decrease on the magnetospheric side of the potential drop.

[21] Figure 3 shows the normalized average parallel velocities of the hot and cold electrons, as well as the normalized field-aligned potential and mirror ratio. There is a clear increase in the average parallel velocity of the cold electrons at the location of the potential drop, because the thermal energy of the magnetospheric cold electron population is less than the magnitude of the ambipolar potential. Therefore, the parallel energy gained by the cold electrons that pass through the acceleration region is significant compared to their parallel energy at the top of the acceleration region. Conversely, as the strength of the ambipolar potential is significantly less than the thermal energy of the hot electrons, there is no significant increase in their average parallel velocity.

[22] When a smoothly varying field-aligned potential structure is enforced, there exists a net potential drop of ~16.8 V between the ionosphere and the magnetosphere. This profile is attained by off-setting the potential at the ionospheric end of the flux tube to match that of the maximum magnetospheric ambipolar potential. As there is no longer a narrow acceleration region at high latitudes, the magnetospheric cold electrons are not accelerated near the ionosphere, and hence the field-aligned current density is decreased from the 0 V net potential drop configuration. It is thus worth noting that the minimum field-aligned current density presented here does not correspond to a 0 V net potential drop between the ionosphere and magnetosphere, but rather to a smoothly varying potential profile between the two regions.

[23] Tables 3 and 4 summarize, for the flux tubes intersecting 4 R_S and 9 R_S, respectively, the net potential drops between the ionosphere and magnetosphere, the corresponding field-aligned current densities at the ionospheric end of the flux tube, and the precipitating electron energy fluxes at the ionosphere. Figure 4 displays the current-voltage relationship for the 9 R_S case for net potential drops of 0.1 V and greater. Our numerical results are denoted with diamonds linked by a dashed line. The solid and dotted lines are analytic relations where the strength of the potential drop is determined between the top of the acceleration region and the ionosphere, and between the equatorial plane and the ionosphere, respectively. These are discussed in further detail in section 4. Clearly, the field-aligned current density increases with net potential drop. Both the hot and cold electrons contribute to the total field-aligned current density, though the cold electrons carry the majority of the current owing to their larger number density. However, as the net potential increases, and the cold electrons are boosted into the loss cone, the contribution from the cold electrons begins to saturate and the relative contribution from the hot electrons increases. This is evidenced by the bump in the current-voltage profile at ~700 V. We do not consider net potential drops larger than 10 kV in our analysis as, in the absence of strong methane absorption lines in the sub-main auroral UV emissions, it is unlikely that such large potential drops would exist in Saturn's middle magnetosphere [*Gustin et al*., 2009; *Grodent et al*., 2010].

4. Analytic Relation

[24] *Knight* [1973] derived an expression for the current-voltage relation of a Maxwellian plasma with a monotonic potential between the ionosphere and plasma sheet in a

Table 3. Net Potential Drops (in V), Ionospheric Current Densities (in μA m^{-2}), and Incident Energy Fluxes (in mW m^{-2}) for the 4 R_S Case

$\Phi_\parallel$	$J_{\parallel i}$	EF
0	1.514	0.00487
−1.8	1.644	0.00466
−3.2	1.752	0.00535
−5.6	1.933	0.00644
−10	2.208	0.00931
−15	2.456	0.0120
−24	2.863	0.0195
−37	3.249	0.0301
−57	3.616	0.0512
−88	3.913	0.0888
−136	4.113	0.158
−210	4.233	0.278
−324	4.285	0.501
−500	4.310	0.916

Table 4. Net Potential Drops (in V), Ionospheric Field-aligned Current Densities (in nA m^{-2}); Total, Cold and hot Electron Contributions, and Incident Electron Energy Fluxes (in mW m^{-2}) for the 9 R_S Case.

$\Phi_\parallel$	$J_{\parallel i}$	$J_{\parallel i_c}$	$J_{\parallel i_h}$	EF
16.8	54.5	37.6	17.0	0.0157
0	96.6	79.5	17.2	0.0164
−1	98.9	81.8	17.3	0.0164
−2.5	103	85.3	17.3	0.0164
−6.3	111	93.9	17.4	0.0165
−16	133	116	17.5	0.0170
−40	175	157	17.9	0.0182
−100	273	255	18.9	0.0224
−250	395	374	21.4	0.0339
−630	471	444	27.5	0.0798
−1585	499	457	41.3	0.255
−3980	530	462	68.2	0.962
−10,000	572	467	105	3.91

steady state, finding that the field-aligned current density increases with the strength of the parallel electric field until the entire electron distribution is shifted into the loss cone, at which point the current density saturates. His analysis assumed that the motion of the particles is dictated by magnetic mirror forces and that the potential structure between the ionosphere and magnetosphere is monotonic. *Ray et al*. [2009] showed that in a rapidly rotating magnetosphere with a centrifugally confined plasma sheet, the top of the acceleration region is located near the minimum in the sums of the gravitational and centrifugal potentials, and hence, the *Knight* [1973] current-voltage relation must be evaluated at high magnetic latitudes along the magnetic flux tube, such that

$$j = j_x + j_x(R_x - 1)\left(1 - e^{-\left(\frac{e\Phi}{k_B T_x (R_x - 1)}\right)}\right) \quad (2)$$

where $j_x = en_x\sqrt{\frac{T_x}{2\pi m_e}}$ is the electron thermal current density, R_x is the magnetic mirror ratio defined at the top of the acceleration region, T_x is the electron temperature expressed in units of energy, n_x is the electron density at the top of the acceleration region, Φ is the magnitude of the potential drop, and e is the fundamental charge of the electron. All quantities with subscript x, along with Φ, are evaluated at the top of the acceleration region.

[25] Our results are consistent with those found by *Ray et al*. [2009] for the Jovian system, owing to similar centrifugal stresses at Saturn. However, because of the smaller magnitude of field-aligned potentials present in Saturn's middle magnetosphere, the strength of the ambipolar potential must be explicitly considered when applying the current-voltage relation. When a 0 V net potential drop is prescribed between the ionospheric and the magnetospheric boundaries, the potential drop from the top of the acceleration region to the ionosphere is found to be ~17 V. It is relative to this value that Φ in equation (2) is evaluated, yielding the current-voltage relation shown in solid line in Figure 4. If, instead, the net potential drop between the ionosphere and magnetosphere is used, as shown with the dotted line in Figure 4, the estimated field-aligned current density is nearly a factor of two less than that found in the numerical simulations. Therefore, the numerical result for a 0 V net potential drop between the ionosphere and the magnetosphere does not yield the expected thermal field-aligned current density, $j_{iono} = R_x j_x$ whereas the results are in agreement when the magnetospheric and ionospheric ambipolar potentials match at high latitudes, such that there exists a net potential drop of ~16.8 V.

[26] The analytic curves in Figure 4 show the summation of the field-aligned current density provided by the hot and cold electron populations, $j = j_c + j_h$, where the independent contributions j_c and j_h are found using equation (2). The top of the acceleration region is taken to be at ~2.3 R_S along the field, yielding a mirror ratio of $R_x = 12$. At this location, the cold electron population can be approximated as a Maxwellian with $n_c = 0.33$ cm^{-3}, $T_c = 18$ eV to represent the tail of the cold Kappa population specified at the magnetosphere. The properties of the hot electrons at the top of the acceleration region are $n_h = 0.018$ cm^{-3} and $T_h = 1$ keV.

[27] In the Jovian system, the potential drops inferred from UV observations of the Io flux tube are ~1 kV, much larger than the magnitude of the ambipolar potential drop, ~125 V. Therefore, for simplicity, the magnitude of the ambipolar potential can be ignored in the analytic expressions. Additionally, the strength of the ambipolar potentials in the Jovian system, relative to the cold electron population's core temperature of 5 eV [*Stefflet al*., 2004], allows a simpler description of the current-voltage relation which solely includes the contribution of the hot electrons. At Saturn, the lack of strong UV emissions at planetary latitudes conjugate with the middle magnetosphere prevents such assumptions. Additionally, the larger abundance of protons in the Saturnian system results in reduced ambipolar electric field strengths, such that the cold electrons reach high magnetic latitudes, carrying a significant fraction of the field-aligned currents.

[28] The contribution of the cold electrons to the field-aligned current density saturates at $\Phi \sim 1$kV, with the hot electrons responsible for the increase in the field-aligned current density at higher voltage drops. Figure 4 does not

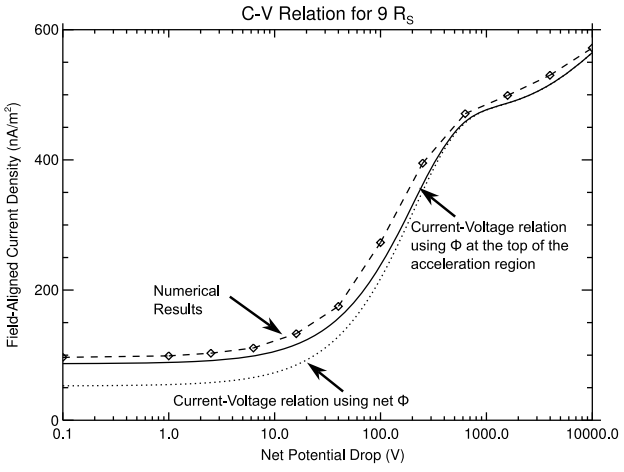

Figure 4. Current-voltage relation for the flux tube intersecting 9 R_S. The dashed line with diamonds shows our numerical results. The solid line is the analytic relation including the ambipolar potential as well as the net potential drop between the ionosphere and the equatorial magnetosphere. The dotted line displays the current-voltage relation without the ambipolar potential.

show the saturation of the field-aligned current density as this occurs for potential drops larger than 10 kV. However, the location of the acceleration region remains nearly fixed across the investigated potential drops; thus, we can infer that the field-aligned current density saturates for $\Phi \geq \sim 50$ kV.

5. Discussion

[29] At Saturn, the rapid rotation of the magnetosphere coupled with a cold, dense internal source of plasma yields an equatorially confined plasma sheet with a scale height of ~2 R_S [*Thomsen et al*., 2010]. The field-aligned density of water group ions, owing partially to their temperature anisotropy and partially to their larger mass, falls off more sharply with distance from the equator than that of the protons. Electrons, less affected by the centrifugal potential, move more freely along the magnetic field lines, and an ambipolar electric field develops to maintain quasineutrality along the magnetic flux tube. At 9 R_S, the strength of this potential drop is ~17 V.

[30] The magnitude of the ambipolar potential drop remains fairly constant with changes in the net potential drop between the ionosphere and the magnetosphere. However, as the net potential drop between the two regions is increased, the field-aligned current density at the ionosphere grows. We find that the relationship between the field-aligned current density and field-aligned potential drop is consistent with that predicted by *Knight* [1973], but only when the plasma parameters are evaluated at the top of the acceleration region. For all simulations, the acceleration forms at ~1.5 R_S along the magnetic field as measured from the center of the planet. Despite increases in the net potential drop, the location of the acceleration region remains constant. However, the density depletion and width of the cavity is increased with net potential drop.

[31] For Saturn, we find similar results to the study by *Ray et al*. [2009] applied to Jupiter; that is, the current-voltage relation must be evaluated at the top of the acceleration region. In both systems, the acceleration region forms at high magnetic latitudes, ~1.5–3 planetary radii along the field as measured from the center of the planet, coincident with the minimum in the sums of the gravitational and centrifugal potentials. However, the strength of the ambipolar potentials in the Saturnian system is less than that at Jupiter, owing to the larger relative abundance of protons in Saturn's magnetosphere. Unlike the Jovian system, which is based in sulfur dioxide chemistry, the water group chemistry—and subsequent proton population—of the Saturnian system helps maintain quasi-neutrality along the flux tube. As a consequence, the magnetospheric electron population is less confined to the equatorial plane by the ambipolar potentials, and a significant fraction of the field-aligned current density is carried by cold electrons. This is consistent with *Su et al*. [2003], who found that the presence of magnetospheric protons has a large effect on the magnitude of the ambipolar potentials, and subsequent ionospheric field-aligned currents and incident energy fluxes in the Jovian system. However, the current-voltage relation described in this analysis differs from that found by *Matsuda et al*. [2012] for the Io wake region at Jupiter. Using a quasistatic multimagnetofluid simulation, they found that the top of the auroral acceleration region shifts with temporal changes in the ionospheric proton density, modifying the ionospheric field-aligned current density, while the net voltage drop across the auroral cavity remains nearly constant.

[32] A faint UV emission has been detected at the base of the Enceladus flux tube with brightnesses ranging from 450 ± 290 Rayleighs to 1550 ± 340 Rayleighs [*Pryor et al*., 2011]. An incident energy flux of 1 mW/m^2 produces 10 ± 0.2 kiloRayleighs of H_2 UV emission in a pure H_2 atmosphere [*Gerard and Singh*, 1982]. Assuming this conversion rate, the associated energy fluxes range from 0.045 mW/m^2 to 0.155 mW/m^2, which corresponds to a net field-aligned potential drop between the ionosphere and magnetosphere of 50–130 V as shown in Table 3. For the flux tube intersecting the equatorial plane at 9 R_S, we find that a net potential drop of 1585 V is consistent with the energy flux of 0.3 mW/m^2 inferred from the diffuse nightside UV emission [*Grodent et al*., 2010] (see Table 4).

[33] At the outer planets, the radial outflow of material through the magnetosphere requires the transport of angular momentum from the planetary atmosphere to the magnetosphere. Assuming a steady-state current system, high-latitude field-aligned potentials develop on magnetic field lines where the thermal field-aligned current density is exceeded, also known as the critical current condition [*Ray et al*., 2010]. In the Jovian system, the field-aligned currents transferring angular momentum from the ionosphere to the magnetosphere surpass the thermal field-aligned current density on flux tubes that intersect the equatorial plane at ~15 R_J. However, the larger percentage of protons in the Saturnian magnetospheric plasma population may result in a magnetosphere in which the critical current condition is never met. *Ray et al*. [2012] found that a magnetospheric plasma population with a larger fraction of hot electrons (3% [*Schippers*, 2009] versus the 0.3% applied in this analysis [*Schippers et al*., 2012]) produces an energy flux of ~0.35 mW/m^2, ionospheric field-aligned current density of 0.318 μA/m^2, and ionospheric Pedersen conductances of ~18.6–18.9 mho for a net voltage of 0 V between the ionosphere and magnetosphere at 9 R_S. For such conditions, it is likely that sufficient angular momentum can be communicated between the planetary atmosphere and magnetosphere without the development of field-aligned potentials and UV auroral emissions. If the diffuse nightside UV auroral emission is driven by a steady-state current system, the local time dependence of the emission suggests that the magnetospheric plasma population varies with local time, such that the nightside hot electron population is fractionally smaller than the dayside. In either case, the energy deposited into the planetary atmosphere may be related to IR auroral emissions.

[34] Additionally, *Cowley and Bunce* [2003] found that the field-aligned currents in Saturn's middle magnetosphere are insufficient to drive bright UV auroral emissions. However, their analysis imposed a radial magnetospheric angular velocity profile to determine the magnitude of the field-aligned currents. Understanding the composition of the magnetospheric plasma, along with the radial mass transport rates and mass-loading rates, is essential in determining the physical processes driving Saturn's middle magnetosphere and auroral emissions. To date, 1-D models have had difficulty reproducing the observed angular velocity profile using the mass-loading rates, radial mass transport rates, and Pedersen conductances inferred from in situ and remote

measurements [e.g., *Saur et al*., 2004; *Pontius and Hill*, 2009]. Therefore, the associated field-aligned currents may also not be well understood. An interesting extension to this study would be to explore the radial evolution of the field-aligned currents including a latitudinally varying Pedersen conductance, radially varying thermal current density, and the possible development of field-aligned potentials.

6. Conclusions

[35] Auroral emissions associated with processes occurring in Saturn's middle magnetosphere are not yet completely understood. The low auroral intensity and lack of hydrocarbon absorption in the Enceladus auroral spot prevent the estimation of the precipitating auroral electron energy from observations. Poleward of the Enceladus spot, there exists a diffuse, auroral emission on the nightside which is magnetically conjugate with distances from 4 to 11 R_S. We applied a 1-D spatial and 2-D velocity space Vlasov code to the flux tubes that intersect Saturn's equatorial plane at 4 and 9 R_S to study the nature of the current-voltage relation at these locations and the associated electron energy flux at the ionosphere. We find the following conclusions:

[36] 1. The magnitude of the magnetospheric ambipolar potentials in the Saturnian system is small owing to the large abundance of protons in the system. As a result, the cold electrons carry most of the field-aligned current density for net potential drops less than ~500 V.

[37] 2. Owing to the strong centrifugal forces, there is a lack of plasma at high latitudes and an auroral cavity develops at ~1.5 R_S along the magnetic field as measured from the center of the planet. The current-voltage relation should be evaluated at this location.

[38] 3. At 4 R_S, field-aligned potentials of ~50 to 130 V, yielding precipitating electrons of 50–130 eV and incident energy fluxes of ~0.05–0.16 mW m^{-2}, are consistent with the Enceladus UV emission.

[39] 4. At 9 R_S, a field-aligned acceleration of ~1.5 kV is required to produce ionospheric electron energy fluxes of 0.3 mW $m^{(-2)}$ for a magnetospheric electron population with a small percentage (0.3%) of hot electrons.

[40] **Acknowledgments.** L.C.R. and M.G. are supported by the Science and Technology Facilities Council (STFC) rolling grant to Imperial College London and NSF IRFP Grant #1064635. L.C.R. received travel support from the RAS. B. F. is supported through the NASA NESSF program. We thank Ingo Mueller-Wodarg very much for very helpful discussions.

References

Achilleos, N., C. S. Arridge, C. Bertucci, C. M. Jackman, M. K. Dougherty, K. K. Khurana, and C. T. Russell (2008), Large-scale dynamics of Saturn's magnetopause: Observations by Cassini, *J. Geophys. Res.*, *113*, A11209, doi:10.1029/2008JA013265.

Alexeev, I. I., V. V. Kalegaev, E. S. Belenkaya, S. Y. Bobrovnikov, E. J. Bunce, S. W. H. Cowley, and J. D. Nichols (2006), A global magnetic model of Saturn's magnetosphere and a comparison with Cassini SOI data, *Geophys. Res. Lett.*, *33*, L08101, doi:10.1029/2006GL025896.

Boström, R. (2003), Kinetic and space charge control of current flow and voltage drops along magnetic flux tubes: Kinetic effects, *J. Geophys. Res.*, *108*(A4), 8004, doi:10.1029/2002JA009295.

Bunce, E. J., S. W. H. Cowley, I. I. Alexeev, C. S. Arridge, M. K. Dougherty, J. D. Nichols, and C. T. Russell (2007), Cassini observations of the variation of Saturn's ring current parameters with system size, *J. Geophys. Res.*, *112*, A10202, doi:10.1029/2007JA012275.

Bunce, E. J., et al. (2008), Origin of Saturn's aurora: Simultaneous observations by Cassini and the Hubble Space Telescope, *J. Geophys. Res.*, *113*, A09209, doi:10.1029/2008JA013257.

Connerney, J. E. P., M. H. Acuña, and N. F. Ness (1983), Currents in Saturn's magnetosphere, *J. Geophys. Res.*, *88*(A11), 8779–8789, doi:10.1029/JA088iA11p08779.

Cowley, S. W. H., and E. J. Bunce (2003), Corotation-driven magnetosphere-ionosphere coupling currents in Saturn's magnetosphere and their relation to the auroras, *Ann. Geophys.*, *21*, 1691–1707.

Dors, E. E., and C. A. Kletzing (1999), Effects of suprathermal tails on auroral electrodynamics, *J. Geophys. Res.*, *104*(A4), 6783–6796, doi:10.1029/1998JA900135.

Dougherty, M. K., et al. (2004), The Cassini Magnetic Field Investigation, *Space Sci. Rev.*, *114*, 331–383.

Dougherty, M. K., et al. (2005), Cassini Magnetometer Observations During Saturn Orbit Insertion, *Science*, *307*, 1266–1270.

Ergun, R. E., et al. (1998), FAST satellite observations of electric field structures in the auroral zone, *Geophys. Res. Lett.*, *25*, 2025–2028, doi:10.1029/98GL00635.

Ergun, R. E., C. W. Carlson, J. P. McFadden, F. S. Mozer, and R. J. Strangeway (2000), Parallel electric fields in discrete arcs, *Geophys. Res. Lett.*, *27*, 4053–4056, doi:10.1029/2000GL003819.

Fleshman, B. L., P. A. Delamere, and F. Bagenal (2010), A sensitivity study of the Enceladus torus, *J. Geophys. Res.*, *115*, E04007, doi:10.1029/2009JE003372.

Galand, M., and S. Chakrabarti (2002), Auroral Processes in the Solar System, p. 55.

Gérard, J.-C., and V. Singh (1982), A model of energy deposition of energetic electrons and EUV emission in the Jovian and Saturnian atmospheres and implications, *J. Geophys. Res.*, *87*(A6), 4525–4532, doi:10.1029/JA087iA06p04525.

Grodent, D., J. Gérard, A. Radioti, B. Bonfond, and A. Saglam (2008), Jupiter's changing auroral location, *J. Geophys. Res.*, *113* A01206, doi:10.1029/2007JA012601.

Grodent, D., A. Radioti, B. Bonfond, and J.-C. Gérard (2010), On the origin of Saturn's outer auroral emission, *J. Geophys. Res.*, *115*, A08219, doi:10.1029/2009JA014901.

Gustin, J., J.-C. Gérard, W. Pryor, P. D. Feldman, D. Grodent, and G. Holsclaw (2009), Characteristics of Saturn's polar atmosphere and auroral electrons derived from HST/STIS, FUSE and Cassini/UVIS spectra, *Icarus*, *200*, 176–187.

Kliore, A. J., A. F. Nagy, E. A. Marouf, A. Anabtawi, E. Barbinis, D. U. Fleischman, and D. S. Kahan (2009), Midlatitude and high-latitude electron density profiles in the ionosphere of Saturn obtained by Cassini radio occultation observations, *J. Geophys. Res.*, *114*, A04315, doi:10.1029/2008JA013900.

Knight, S. (1973), Parallel electric fields, *Planet. Space Sci.*, *21*, 741–750.

Lewis, G. R., et al. (2010), The calibration of the Cassini-Huygens CAPS Electron Spectrometer, *Planet. Space Sci.*, *58*, 427–436.

Lyons, L. (1980), Generation of large-scale regions of auroral currents, electric potentials, and precipitation by the divergence of the convection electric field, *J. Geophys. Res.*, *85*(A1), 17–24, doi:10.1029/JA085iA01p00017.

Matsuda, K., N. Terada, Y. Katoh, and H. Misawa (2012), A simulation study of the current–voltage relationship of the Io tail aurora, *J. Geophys. Res.*, *117*, A10214, doi:10.1029/2012JA017790.

McFadden, J. P., C. W. Carlson, and R. E. Ergun (1999), Microstructure of the auroral acceleration region as observed by FAST, *J. Geophys. Res.*, *104*(A7), 14453–14480, doi:10.1029/1998JA900167.

Mella, M. R., K. A. Lynch, D. L. Hampton, H. Dahlgren, P. M. Kintner, M. Lessard, D. Lummerzheim, E. T. Lundberg, M. J. Nicolls, and H. C. Stenbaek-Nielsen (2011), Sounding rocket study of two sequential auroral poleward boundary intensifications, *J. Geophys. Res.*, *116*, A00K18, doi:10.1029/2011JA016428.

Mozer, F. S., and C. A. Kletzing (1998), Direct observation of large, quasi-static, parallel electric fields in the auroral acceleration region, *Geophys. Res. Lett.*, *25*, 1629–1632.

Paschmann, G., S. Haaland, and R. Treumann (2003), Auroral Plasma Physics, in *Reprinted from Space Science Reviews* Vol. *103*, edited by G. Paschmann, International Space Science Institute, Bern Switzerland, and Max-Planck-Institut fuer Extraterrestrische Physik, Garching, Germany; S. Haaland, International Space Science Institute, Bern Switzerland and Max-Planck-Institut fuer Extraterrestrische Physik, Garching, Germany; R. Treumann, Max-Planck-Institut fuer Extraterrestrische Physik, Garching, Germany, pp. 1–4, 2002 Kluwer Academic Publishers, Dordrecht.

Pontius, D. H., and T. W. Hill (2009), Plasma mass loading from the extended neutral gas torus of Enceladus as inferred from the observed plasma corotation lag, *Geophys. Res. Lett.*, *36*, L23103, doi:10.1029/2009GL041030.

Pryor, W. R., et al. (2011), The auroral footprint of Enceladus on Saturn, *Nature*, *472*.

Ray, L. C., Y. Su, R. E. Ergun, P. A. Delamere, and F. Bagenal (2009), Current–voltage relation of a centrifugally confined plasma, *J. Geophys. Res.*, *114*, A04214, doi:10.1029/2008JA013969.

Ray, L. C., R. E. Ergun, P. A. Delamere, and F. Bagenal (2010), Magnetosphere-ionosphere coupling at Jupiter: Effect of field-aligned potentials on angular momentum transport, *J. Geophys. Res.*, *115*, A09211, doi:10.1029/2010JA015423.

Ray, L. C., M. Galand, L. E. Moore, and B. L. Fleshman (2012), Characterizing the limitations to the coupling between Saturn's ionosphere and middle magnetosphere, *J. Geophys. Res.*, *117*, A07210, doi:10.1029/2012JA017735.

Saur, J., F. M. Neubauer, J. E. P. Connerney, P. Zarka, and M. G. Kivelson (2004), Plasma interaction of Io with its plasma torus, pp. 537–560.

Schippers, P. (2009), Etude de l'équilibre et de la circulation des populations d'électrons dans la magnétosphère de Saturne à l'aide des données multi-instrumentales de la sonde Cassin-Huygens, Ph.D. thesis, L'Université de Toulouse.

Schippers, P., et al. (2008), Multi-instrument analysis of electron populations in Saturn's magnetosphere, *J. Geophys. Res.*, *113*, A07208, doi:10.1029/2008JA013098.

Schippers, P., N. André, D. A. Gurnett, G. R. Lewis, A. M. Persoon, and A. J. Coates (2012), Identification of field-aligned currents in Saturn's magnetosphere, *J. Geophys. Res.*, *117*, A05204, doi:10.1029/2011JA017352.

Sittler, E. C., et al. (2008), Ion and neutral sources and sinks within Saturn's inner magnetosphere: Cassini results, *Planet. Space Sci.*, *56*, 3–18.

Stallard, T., et al. (2008), Complex structure within Saturn's infrared aurora, *Nature*, *456*, 214–217.

Stallard, T., H. Melin, S. W. H. Cowley, S. Miller, and M. B. Lystrup (2010), Location and Magnetospheric Mapping of Saturn's Mid-latitude Infrared Auroral Oval, *The Astrophys. J. Lett.*, *722*, L85–L89.

Steffl, A. J., F. Bagenal, and A. I. F. Stewart (2004), Cassini UVIS observations of the Io plasma torus. II. Radial variations, *Icarus*, *172*, 91–103.

Su, Y.-J, R. E. Ergun, F. Bagenal, and P. A. Delamere (2003), Io-related Jovian auroral arcs: Modeling parallel electric fields, *J. Geophys. Res.*, *108*(A2), 1094, doi:10.1029/2002JA009247.

Thomsen, M. F., D. B. Reisenfeld, D. M. Delapp, R. L. Tokar, D. T. Young, F. J. Crary, E. C. Sittler, M. A. McGraw, and J. D. Williams (2010), Survey of ion plasma parameters in Saturn's magnetosphere, *J. Geophys. Res.*, *115*, A10220, doi:10.1029/2010JA015267.

Wannawichian, S., J. T. Clarke, and D. H. Pontius (2008), Interaction evidence between Enceladus' atmosphere and Saturn's magnetosphere, *J. Geophys. Res.*, *113*, A07217, doi:10.1029/2007JA012899.

Wilson, R. J., R. L. Tokar, M. G. Henderson, T. W. Hill, M. F. Thomsen, and D. H. Pontius (2008), Cassini plasma spectrometer thermal ion measurements in Saturn's inner magnetosphere, *J. Geophys. Res.*, *113*, A12218, doi:10.1029/2008JA013486.